A set of methods to evaluate the below-cloud evaporation effect on local precipitation isotopic composition: a case study in Xi'an, China

Meng Xing[1,2*], Weiguo Liu[1,2,3*], Jing Hu[1,2], Zheng Wang[1,2]

1. State Key Laboratory of Loess and Quaternary Geology, Institute of Earth Environment, Chinese Academy of Sciences, Xi'an, 710061, China

2. CAS Center for Excellence in Quaternary Science and Global Change, Xi'an, 710061, China.

3. University of Chinese Academy of Sciences, Beijing, 100049, China

Corresponding authors:

Meng Xing email address: xingmeng@ieecas.cn

Weiguo Liu email address: liuwg@loess.llqg.ac.cn

Abstract:

When the hydrometeor falls from the in-cloud saturated environment towards the ground, especially in the arid and semi-arid regions, the below-cloud processes could heavily alter the precipitation isotopic composition through equilibrium and non-equilibrium fractionations, and accounts for the misinterpretation of precipitation isotopic signal if these processes cannot be properly identified. To correctly understand the environmental information contained in the precipitation isotopes, qualitatively analyzing the below-cloud processes and quantitatively calculating the below-cloud evaporation effect are becoming very important. Here, based on a two-year synchronous observations of precipitation and water vapor isotopes in Xi'an, we compiled a set of effective methods to systematically evaluate the below-cloud evaporation effect on local precipitation isotopic composition. The ΔdΔδ-diagram shows the isotopic differences (δ^2H, d-excess) of the precipitation-equilibrated vapor relative to the observed vapor, in which the equilibration and evaporation could lead to different pathways in the two-dimensional phase space. By using ΔdΔδ-diagram, our data show that evaporation is the major below-cloud process, while snowfall samples retain the initial cloud signal because of less isotopic exchange between vapor and solid phases. To quantitatively characterize the influence of below-cloud evaporation on precipitation isotopic composition, here, we chose two methods: one is based on the raindrop's mass change during its falling (hereafter referred to as method 1); another is to directly calculate the precipitation isotopic variations from the cloud base to the ground (hereafter referred to as method 2). By comparison, we found that there are no statistical differences between the two methods in evaluating the evaporation effect on δ^2H_p, except for snowfall events. The slope of evaporation proportion and difference in δ^2H ($F_i/\Delta\delta^2H$) is a little larger in method 1 (1.0 ‰/%) than in method 2 (0.9 ‰/%). Additionally, both methods indicate that the raindrops are weakly evaporated in autumn, and heavily evaporated in spring. Through the sensitivity test, relative humidity is the most sensitive parameter in both, while the variations of temperature show different effects on the two methods. Therefore, following our methods, the diagnosis of below-cloud processes and the understanding of their effects on the precipitation isotopic composition will be improved.

1 Introduction

For the paleoenvironment, the isotopic signal of precipitation recorded in ice cores (Thompson et al., 2000; Yao et al., 1996), tree rings (Liu et al., 2004; Liu et al., 2017b), speleothems (Cai et al., 2010; Tan et al., 2014), and leaf wax of loess-paleosol deposits (Wang et al., 2018b) and lake sediments (Liu et al., 2017a, 2019) could be used to reconstruct the information of temperature, precipitation, and hydrological regimes in geologic history, as it had participated into the formation or the growth of these geological archives. For the modern environment, it could be used to quantitatively constraint the water vapor contribution from the end-members of advection (Peng et al., 2011), evaporation (Sun et al., 2020; Wang et al., 2016a), transpiration (Li et al., 2016; Zhao et al., 2019), and even anthropogenic activities (Fiorella et al., 2018; Gorski et al., 2015; Xing et al., 2020), as itself is an important part of the hydrological cycle. Thus, the hydrogen and oxygen isotopes of precipitation are one of the most important tools to trace the hydrological cycle and climate change (Bowen et al., 2019; Gat, 1996). However, limited by the sampling and isotopic fractionation theories, there remains large uncertainty (i.e., the below-cloud evaporation intensity, the moisture recycling ratio, water molecules exchange between the droplet and ambient air, etc.) in deciphering the information contained in precipitation by using hydrogen and oxygen isotopes (Bowen et al., 2019; Yao et al., 2013).

Below-cloud evaporation is exactly one of the processes that influence the falling raindrops, modify their final stable isotopic content, and thus needs to be properly evaluated. Over the past decades, to determine whether the hydrometeor has been evaporated during its falling, most studies depend on a second-order isotopic parameter (Dansgaard, 1964; Jeelani et al., 2018; Li and Garzione, 2017), deuterium excess (defined as d-excess= $\delta^{2}H-8\times\delta^{18}O$). This parameter is representative of the non-equilibrium fractionations, since light isotopes (^{1}H and ^{16}O) equilibrate faster than heavy isotopes (^{2}H and ^{18}O) in different phases (Clark and Fritz, 1997; Dansgaard, 1964). For raindrops, the lighter water molecules ($^{1}H_{2}{}^{16}O$) preferentially equilibrate or diffuse from the liquid phase to the gas phase during their falling through unsaturated ambient air. The equilibrium fractionation would not change the d-excess, while the non-equilibrium diffusional process would result in a decrease of d-excess in rain (Fisher, 1991; Merlivat and Jouzel, 1979). Additionally, the slope of the local meteoric water line (LMWL) has also been widely used as a metric to infer the below-cloud evaporation effect according to the theory of water isotope equilibrium fractionation

(Chakraborty et al., 2016; Putman et al., 2019b; Wang et al., 2018a). Generally, the LMWL's slope is approximately equal to 8.0 belonging to equilibrium fractionation and that is lower than 8.0 pointing to a non-equilibrium fractionation, such as the re-evaporation of raindrops.

However, it is worth noting that the change of air masses (Guan et al., 2013), the condensation in supersaturation conditions (Jouzel et al., 2013), or the moisture exchange in the cloud and sub-cloud layer (Graf et al., 2019) also cause large variations in the slopes and d-excess values (Putman et al., 2019a; Tian et al., 2018). Therefore, it is imperative to explore a novel method to more accurately identify the below-cloud evaporation process. Recently, Graf et al. (2019) provided a new interpretive framework to directly separate the convoluted influences on the stable isotopic composition of vapor and precipitation according to the theoretical fractionation processes, especially the influences of equilibration and below-cloud evaporation. The axes of the new diagram consist of the differences, $\Delta\delta^2H$ and Δd, between the isotopic composition of precipitation equilibrate vapor and near-surface vapor, namely $\Delta\delta\Delta d$-diagram. Compared with the slope of LMWL or the d-excess, the below-cloud equilibration and evaporation have different spatial distributions in the two-dimensional phase space of $\Delta\delta\Delta d$-diagram, which makes them more easily distinguishable. Although the $\Delta\delta\Delta d$-diagram gives us a new guideline to more accurately identify the below-cloud evaporation, Graf's et al. (2019) work was only tested on a cold frontal rain event during a short time, and hence more works need to be done for validating the general applicability of their framework.

The initial signal of precipitation isotopes is important in hydrological studies, and thus it is necessary to quantitatively evaluate the influence of below-cloud evaporation on its variations. Normally, the isotopic difference of raindrops between ground level and cloud base is determined by the below-cloud evaporation intensity. Due to the difficulty of measuring the vapor or precipitation isotopic composition at the cloud base, the model proposed by Stewart (1975) has been widely used to estimate the below-cloud evaporation effect for a long time. Based on the well-defined laboratory conditions, Stewart (1975) parameterized the change of the isotopic composition of a falling water drop with the vapor and raindrop isotopic compositions at the cloud base, and the remaining fraction of raindrop mass after evaporation (hereafter referred to as method 1). Froehlich et al. (2008) adapted the Stewart model and then assessed the change in d-excess due to below-cloud evaporation based on a simple frame in the European

Alps. Wang et al. (2016b) further refined the calculations of the parameters, which are used to determine the remaining fraction of raindrop mass in the Stewart model, to assess the variation in d-excess of raindrops in central Asia. However, these quantitative evaluations for the below-cloud evaporation are indirect, because the results are largely dependent on the parameter that is the remaining fraction of raindrop mass after evaporation.

In recent years, with the progress in optical laser systems, a relatively portable field-deployable laser spectroscopic instruments have emerged, which makes the online, autonomous, and high-frequency site measurements of the water vapor stable isotope composition to be achieved (Aemisegger et al., 2012; Christner et al., 2018). Therefore, the vapor or precipitation isotopic composition at the cloud base could be directly measured (Salmon et al., 2019), or be indirectly deduced from the ground-level vapor isotopic composition (Deshpande et al., 2010; Salamalikis et al., 2016). This enables us to directly calculate the influence of below-cloud processes on the precipitation isotopic composition (hereafter referred to as method 2). However, less work has systematically compared the two methods.

Here, we use the measurements of two-year near-ground water vapor isotope composition, and 141 precipitation isotope compositions (including event-based snowfall samples)which were collected in Xi'an (34.23°N, 108.88°E), Shaanxi province, located in the Chinese Loess Plateau (CLP). The objectives of this study are to: 1. qualitatively identify the below-cloud processes of falling raindrops by using the ΔδΔd-diagram ; 2. quantitatively evaluate the below-cloud evaporation effect on precipitation isotopic composition by two methods and compare their differences; 3. understand the role of meteorological factors on the below-cloud evaporation and the characteristics of below-cloud evaporation in Xi'an city. Therefore, with the advantages of the paired observations of the vapor and precipitation isotopes near the ground, this study will compile a set of effective methods to evaluate the below-cloud evaporation effect on the local precipitation isotopic composition.

2 Data and methods

2.1 Sampling site

As the capital city of Shaanxi province and the largest city in northwest China, Xi'an is located on the Guanzhong Plain on the southern edge of the CLP at an average elevation of 400 m. The city is located in a semi-arid to arid region and is representative

of most cities in the north and northwest of China (e.g., Lanzhou and Xining city, Fig. 1). The mean annual precipitation is 573.7mm, and the mean annual evaporation is 426.6mm from 1951 to 2008 year (Wu et al., 2013). The notable below-cloud evaporation effect has been reported in many studies for this area (Sun et al., 2020; Wan et al., 2018; Zhu et al., 2016). Therefore, it is an ideal site to study the below-cloud processes.

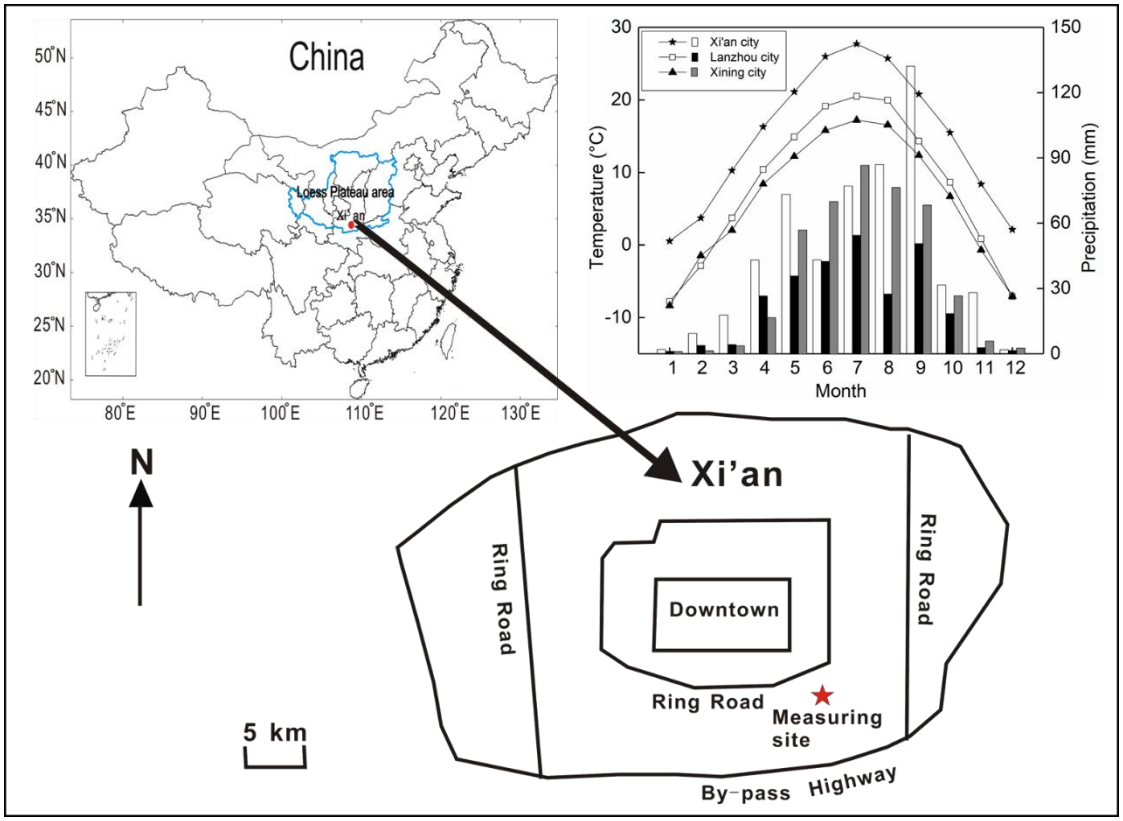

Figure 1 Average monthly variations of temperature and precipitation in Xi'an, Lanzhou, and Xining during 2010-2015. Location of the sampling site in the Yanta Zone, 9 km SE of downtown Xi'an. Water vapor samples are taken on the seventh floor of a twelve-story building, about 30 m above ground level. Precipitation samples are collected on the top floor, 1 m above ground level.

The water vapor in-situ measurement site is located in a residential area, approximately 10 km southeast to downtown of Xi'an city (Fig. 1). The atmospheric water vapor isotopic composition was observed from 1 January 2016 to 31 December 2017 on the seventh floor of the Institute of Earth and Environment, Chinese Academy of Sciences, about 30 m above ground. The rainfall or snowfall collector was placed on the rooftop of the buildings (1 m above the floor of the roof), about 50 m above ground.

2.2 Sampling and isotopic measurement

Rainfall and snowfall samples were collected manually from the beginning of each

precipitation event using a polyethylene collector (700 mm × 450 mm × 170 mm). Before being used, the collector was cleaned with soap and water, rinsed with deionized water, and then dried. When the precipitation event ended, the collector was quickly taken back to minimize water evaporation. The rainfall volume was measured using a graduated flask. After collection, the samples were filtered through 0.40–μm polycarbonate membranes. Then, the rainfall samples were immediately poured into 100 ml polyethylene bottles. The snowfall samples were first melted at room temperature in closed plastic bags, after filtration, and then immediately poured into 100 ml polyethylene bottles. About a 2 ml of each filtrate was transferred into a sample vial, and stored at -4°C until being measured. Of the collected 141 samples, during the two-year sampling campaigns, 130 are rainfall samples and the other 11 are snowfall samples (Table S3).

In all cases, the data are reported in the standard delta notation (δ), i.e., the per mil (‰) deviation from Vienna Standard Mean Ocean Water according to, $\delta = (R_{sample}/R_{reference}-1) \times 1000$, where R is the isotope ratio of the heavy and light isotope (e.g., $^{18}O/^{16}O$) in the sample and the reference.

The precipitation samples were measured with a Picarro L2130-i (serial number HIDS 2104) wavelength-scanned cavity ring-down spectrometer at a high-precision mode. Every isotopic standard or sample was injected sequentially 8 times using a 5 μL syringe, and then the arithmetic average of the last 3 injections was accepted as the final result. All the samples were calibrated by three laboratory standards, while the $\delta^{18}O$ and $\delta^{2}H$ true values of the three laboratory standards (Laboratory Standard-1 (LS-1): $\delta^{18}O$ =+0.3‰, $\delta^{2}H$ =–0.4‰; Laboratory Standard-2 (LS-2): $\delta^{18}O$ =–8.8‰, $\delta^{2}H$ =–64.8‰; Laboratory Standard-3 (LS-3): $\delta^{18}O$ =–24.5‰, $\delta^{2}H$ =–189.1‰) are calibrated to the scale of two international standards VSMOW(Vienna Standard Mean Ocean Water)-GISP(Greenland Ice Sheet Precipitation), with a precision of ±0.2‰ and ±1.0‰, for $\delta^{18}O$ and $\delta^{2}H$, respectively. To correct the instrument drift, the three laboratory standards were repeatedly measured after measuring every 8 samples.

Atmospheric water vapor $\delta^{18}O_v$ and $\delta^{2}H_v$ were also measured by Picarro L2130-i, but at a liquid-vapor dual mode. The inlet of the gas-phase instrument is connected to the vapor source through an external solenoid valve when measuring vapor samples. This valve can switch the input of the instrument from the vapor sample to dry gas. The instrument is connected to dry gas prior to being connected to the evaporator for

measuring liquid water standards so that any traces of the water vapor sample are removed from the measurement cell. The standards are injected into the evaporator with a CTC Analytics autosampler, PAL HTC-xt (Leap Technologies, Carrboro, NC, USA), and measured by the laser spectrometer. The atmospheric water vapor is pumped through a 2 m stainless-steel tube (1/8 inch) using a diaphragm pump at the speed of 4 L min^{-1} and also detected by the laser spectrometer. The outside length of the stainless-steel tube is about 0.5 m, and the inside length is about 1.5 m. We covered the stainless-steel tube with a heating tape maintained at 60 °C to prevent water vapor from condensing in the stainless-steel tube. The air intake was protected with a shield to prevent rainwater from entering the sample line and direct sunlight.

The raw water vapor $\delta^{18}O_v$ and $\delta^{2}H_v$ data were obtained approximately at 1 Hz and then block-averaged into 1 h intervals. As the main usage of this instrument is to measure the liquid water samples in our laboratory, it is used to monitor the water vapor isotopes in its spare time. Thus, the missing data indicate that the instrument is used for measuring liquid samples or being maintained. The event-based water vapor isotopic result is the average value from the start of the precipitation event to the end.

The hourly meteorological data, such as temperature, relative humidity (RH), and surface pressure in Xi'an, are reported by the Chinese meteorological administration, and can be downloaded from the website of http://www.weather.com.cn/. The meteorological station is about 10 km to the north of our sampling site.

2.3 The representativeness of the data

In 2 years, a total of 514 days of water vapor isotopic composition measurements were carried out. For 141 precipitation samples, of which 100 precipitation samples have corresponding event-based water vapor isotopic results. In this study, the precipitation events mainly occurred in summer and autumn, and less in winter and spring. In summer and autumn, the rainfall amount accounted for more than 70% of the annual rainfall (Fig. S3). This is consistent with the multi-year average precipitation distribution in Xi'an (Fig. 1). Therefore, the collected samples are able to represent the precipitation characteristics in this region.

2.4 Water vapor isotopic data correction

Since the water vapor concentration effect and isotopic composition dependency of the cavity ringdown spectrometer have been pointed out by many studies (e.g.,

Bastrikov et al., 2014; Benetti et al., 2014; Steen-Larsen et al., 2013; Weng et al., 2020), it is important to determine the isotopic composition-humidity correction response function. The humidity dependency shown in Fig. S1 also shows a dependency on the isotopic composition of the standards as reported by Weng et al. (2020). For example, in Fig. S1a and Fig. S1b, LS-1 shows a decrease in $\Delta\delta^{18}O$ and $\Delta\delta^{2}H$ with decreasing humidity, while LS-3 shows an increase with decreasing humidity. Therefore, we referred to Weng's et al. (2020) correction scheme for the isotope composition-humidity dependency.

The isotopic measurements of ground-level $\delta^{18}O_v$ and $\delta^{2}H_v$ were corrected for isotopic composition-humidity dependency using:

$$\delta_{meas} - \delta_{iso\text{-}hum\text{-}cor} = \frac{a(\delta_{iso\text{-}hum\text{-}cor})}{h} + b(\delta_{iso\text{-}hum\text{-}cor}) \times h + c(\delta_{iso\text{-}hum\text{-}cor}) \quad \text{(eq. 1)}$$

where $\delta_{iso\text{-}hum\text{-}cor}$ is for isotopic composition-humidity dependency corrected water vapor isotopic composition at 20000 ppmv; δ_{meas} is the raw, measured isotopic composition at that humidity; h is the measured humidity; and a, b, and c are fitting coefficients for each water standard and isotope species. The detailed correction processes are provided in the supplementary material (Appendix A).

To calibrate the measured water vapor isotopic composition to the VSMOW-GISP scale, three known-value laboratory standards have been used in the conversion, while these standards were measured in 24 h intervals to correct for instrument drifts. The 1σ estimated total uncertainties are from 2.1 to 12.4 ‰ for $\delta^{2}H_v$, 0.4 to 1.7 ‰ for $\delta^{18}O_v$, and 3.8 to 18.4 ‰ for d-excess$_v$ over the range of humidity from 30000 to 3000 ppmv on a 10-minutes average through the approach using a Monte Carlo method.

2.5 Analytical methods

2.5.1 ΔdΔδ-diagram

When the raindrop falls from the cloud base to the ground, it continuously exchanges with the surrounding vapor and may lead to net loss due to evaporation. However, this process is very hard to be quantified by observation. Making use of stable water isotopes, Graf et al. (2019) introduced a ΔdΔδ-diagram to diagnose the below-cloud processes and their effects on vapor and precipitation isotopic composition, since equilibration and evaporation are two different processes and lead to different directions in the two-dimensional phase space of the ΔdΔδ-diagram. Here, the differences in the isotopic composition of precipitation-equilibrated vapor relative to the observed ground-level vapor can be expressed as:

$$\Delta\delta_v=\delta_{pv\text{-}eq}-\delta_{gr\text{-}v} \quad \text{(eq. 2)}$$

$$\Delta\text{d-excess}_v=\text{d-excess}_{pv\text{-}eq}-\text{d-excess}_{gr\text{-}v} \quad \text{(eq. 3)}$$

where $\delta_{pv\text{-}eq}$ and $\delta_{gr\text{-}v}$ are the δ^2H ($\delta^{18}O$) of equilibrium vapor from precipitation and observed vapor near the ground, respectively, and d-excess$_{pv\text{-}eq}$ and d-excess$_{gr\text{-}v}$ are d-excess values of equilibrium vapor from precipitation and observed vapor near the ground, respectively. For the detailed calculation processes, please refer to the supplemental material (Appendix B), or Graf et al. (2019).

2.5.2 Below-cloud evaporation calculation: Method 1

As reported by Stewart (1975), the isotopic ratio of a falling water drop is:

$$^iR_{gr} = {}^i\gamma {}^iR_{va} + ({}^iR_{cb} - {}^i\gamma {}^iR_{va})F_r^{\,i\beta} \quad \text{(eq. 4)}$$

where $^iR_{gr}$ is the isotopic ratio of falling raindrops near the ground; $^iR_{va}$ and $^iR_{cb}$ are the initial isotopic ratios for the vapor and raindrop at the cloud base; $^i\gamma$ and $^i\beta$ are the parameters related to equilibrium fractionation factor, relative humidity, and molecular diffusivities; and F_r is the remaining fraction of raindrop mass after evaporation.

Assuming that the initial isotopic composition of the raindrop at the cloud base is in equilibrium with the surrounding water vapor, Froehlich et al. (2008) adapted the Stewart model and simplified the equation to evaluate the isotopic enrichment due to below-cloud evaporation by:

$$\Delta\delta_p=\left(1-\frac{\gamma}{\alpha}\right)(F_r^{\beta}-1) \quad \text{(eq. 5)}$$

$$F_i = (1\text{-}F_r) \times 100\% \quad \text{(eq. 6)}$$

where α is the equilibrium fractionation factor for hydrogen and oxygen isotopes; the parameters of γ and β are defined by Stewart (1975); F_r is the remaining fraction of raindrop mass after evaporation; $\Delta\delta_p$ is the raindrop isotopic variations due to below-cloud evaporation; and F_i is evaporation proportion. For the detailed calculation processes, please refer to the supplemental material (Appendix C), or Froehlich et al. (2008), Wang et al. (2016b), and Salamalikis (2016).

2.5.3 Below-cloud evaporation calculation: Method 2

Because the isotopic composition of a raindrop is directly influenced by the below-cloud processes during its falling, the below-cloud effects could be directly represented by the difference between the isotopic composition of precipitation at the ground level and cloud base:

$$\Delta\delta_p =\delta_{gr\text{-}p}-\delta_{cb\text{-}p} \quad \text{(eq. 7)}$$

where $\delta_{gr\text{-}p}$ and $\delta_{cb\text{-}p}$ are the isotope compositions of a falling raindrop near the ground and below the cloud base, respectively; and $\Delta\delta_p$ is the raindrop isotopic variation due to below-cloud evaporation. The $\delta_{gr\text{-}p}$ is our observed precipitation isotopic composition, and $\delta_{cb\text{-}p}$ is able to calculate based on ground-level water vapor isotopic composition according to Deshpande et al. (2010). For the detailed calculation processes, please refer to the supplemental material (Appendix D), or Araguás-Araguás et al. (2000), Deshpande et al. (2010), and Salamalikis (2016).

Here, it should be noted that in this method we assumed that the raindrop isotopic composition ($\delta_{cb\text{-}p}$) at the cloud base is in equilibrium with the surrounding water vapor, and the observed ground-level precipitation isotopic composition ($\delta_{gr\text{-}p}$) includes the processes of evaporation, growth, and isotopically equilibrium with the surrounding vapor. In addition, during the hydrometeors falling we assumed that there is no horizontal advection into or out of the column, and no updraft or downdraft. The equilibrium exchange process is not separated from the evaporation, therefore, the $\Delta\delta$ results may underestimate the below-cloud evaporation effect in method 2. To get accurate results, more works need to separate the equilibration process from the evaporation in the future.

Actually, method 1 makes use of the mass change of the falling raindrop to evaluate the below-cloud evaporation effect on isotopic composition, while method 2 evaluates its effect by directly measuring the variations of isotope composition.

2.5.4 Statistical Analysis

To compare the difference between the two methods, the independent t-test was performed on SPSS 13.0 (SPSS Inc., Chicago, US). A significant statistical difference was set at $p < 0.05$.

3 Results and discussion

3.1 Relationship between water vapor and precipitation isotopic compositions

Influenced by the below-cloud evaporation, the slope of the local meteoric water line (LMWL) would be lower than 8, the precipitation isotopic composition become more positive, the d-excess of precipitation would be less than 10, and the equilibrated water vapor isotopic composition would be more positive than the observed one. As shown in Fig. 2, the LMWL is: $\delta^2H_p=7.0\times\delta^{18}O_p+3.0$ based on event precipitation isotopic composition, and the local water vapor line (LWVL) is: $\delta^2H_v=7.8\times\delta^{18}O_v+15.1$ based on

per-precipitation-event water vapor isotopic composition. Both the slope and intercept of LMWL are lower than the Global Meteoric Water Line (GMWL) which are 8.0 and 10.0 (Dansgaard, 1964; Gat, 1996), respectively, indicating the potentially significant below-cloud evaporation effect on precipitation (Froehlich et al., 2008). In general, the slopes of the meteoric water lines are indicative of kinetic processes superimposed on the equilibrium fractionation, and the little lower slope of LWVL (slope=7.8) than the expected equilibrium fractionation (slope=8.0) may also relate to the increasing influence of kinetic processes (Rangarajan et al., 2017).

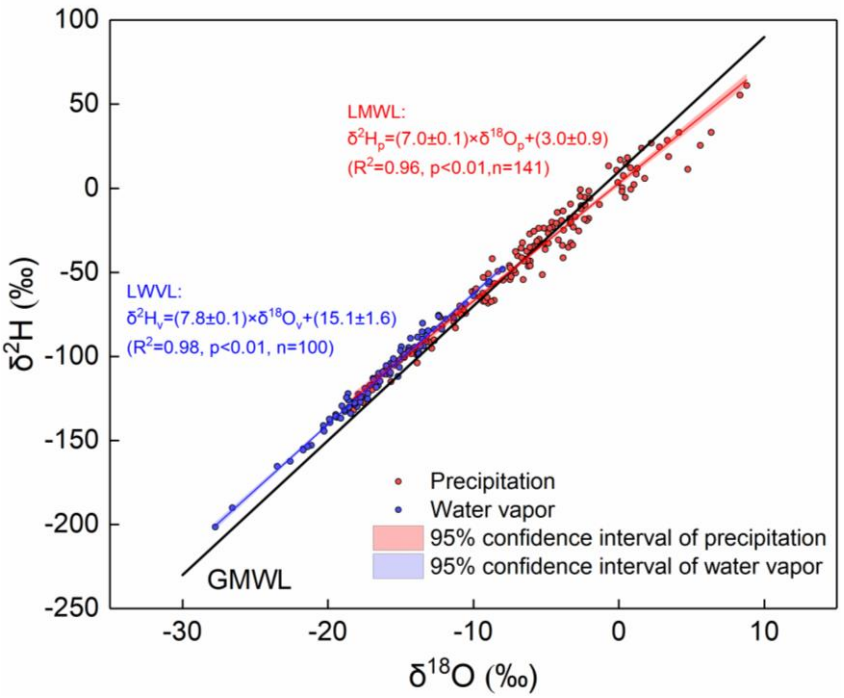

Figure 2 Local meteoric water line (LMWL) and Local water vapor line (LMVL) in Xi'an city.

Besides, we noted that the water vapor and precipitation isotopic composition basically distribute in different range values, which the former is generally more negative than the latter (Fig. 2). According to the classical isotopic fractionation theory, the heavier isotopes preferentially condense into the liquid phase during the precipitation process, which results in the precipitation isotopic composition more positive than the water vapor one (Dansgaard, 1964). Hence, the distribution characteristics of water vapor and precipitation on the $\delta^{18}O$-δ^2H plot would make us suppose that their isotopic compositions are in or close to equilibrium in this study site. To validate our assumption, we plot their relationship in Fig. 3a. As expected, they show a significant positive correlation ($R^2=0.70$, $p<0.01$), and thus the water vapor isotopic composition can explain 70% of the variation of precipitation isotopic composition. Further, we used the measured precipitation isotopic composition to deduce the water vapor isotopic

composition at the ground level according to the liquid-vapor equilibrium isotope fractionation ($\delta^{18}O_{pv\text{-}eq}$), and compared it with observed water vapor ($\delta^{18}O_v$) in Fig. 3b. The scatterplot of the observed $\delta^{18}O_v$ against the equilibrated $\delta^{18}O_{pv\text{-}eq}$ also presents a significantly positive relationship (Fig. 3b).

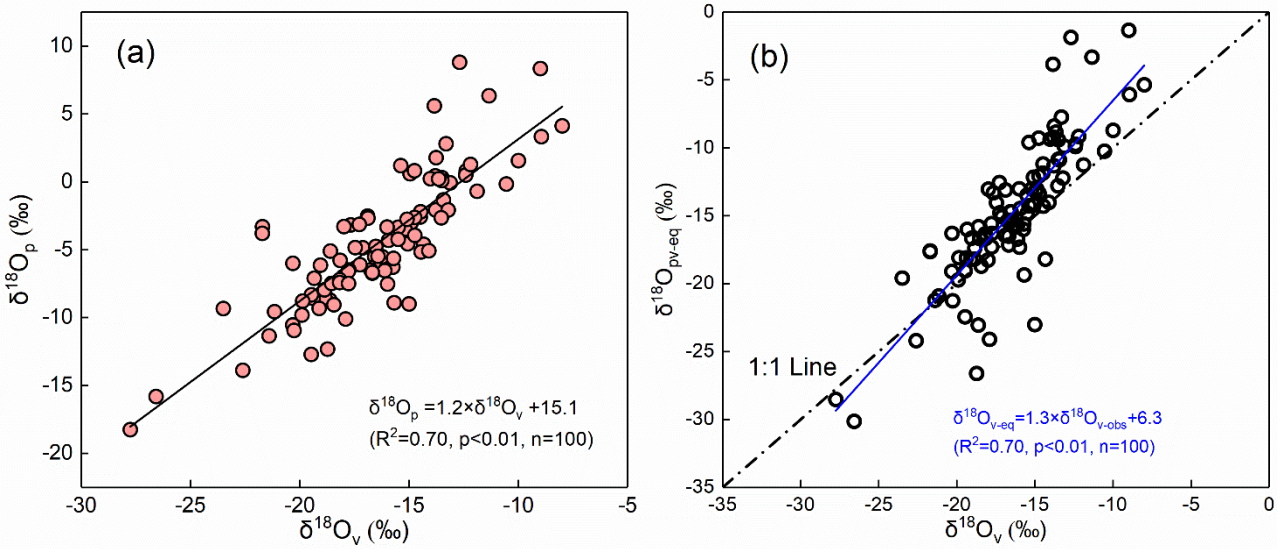

Figure 3 Relationship between $\delta^{18}O_p$ of precipitation and $\delta^{18}O_v$ of water vapor in Xian (a); and the relationship between the equilibrium computed $\delta^{18}O_{pv\text{-}eq}$ based on the precipitation isotopic composition and the near ground observed $\delta^{18}O_v$ (b). The dash-dot line in (b) stands for the 1:1 line, and the blue line represents the regression line of the data.

In the relationship plot, we also noted that the equilibrated $\delta^{18}O_{pv\text{-}eq}$ is relatively more positive than the observed $\delta^{18}O_v$ (Fig. 3b). Because Xi'an city belongs to the semi-arid area, the raindrop is likely to be evaporated in the unsaturated environment during its falling. Therefore, the positive $\delta^{18}O_{pv\text{-}eq}$ is caused by the non-equilibrium fractionation in low relative humidity, which makes the $\delta^{18}O_{pv\text{-}eq}$-$\delta^{18}O_v$ points deviation from the 1:1 line.

The reasonable agreement of observed and equilibrated water vapor isotopic composition has been reported by Jacob and Sonntag (1991), Welp et al. (2008), and Wen et al. (2010), however, they postulated the different relationships underlying the $\delta^{18}O_v$ and $\delta^{18}O_{pv\text{-}eq}$. Jacob and Sonntag (1991) suggested that the water vapor isotopic composition is possible to be deduced from the corresponding precipitation isotopic composition, but Wen et al. (2010) speculated that the equilibrium method cannot accurately predict the ground-level water vapor isotopic composition in arid and semiarid climates because of two monthly equilibrated water vapor values deviating from the observed values. Here, with two-year continuous observation, the mean

difference between the $\delta^{18}O_v$ and $\delta^{18}O_{pv\text{-}eq}$ is −1.1‰ for $\delta^{18}O$, -8.1‰ for $\delta^{2}H$, and 0.7‰ for d-excess. Although there is a good relationship between $\delta^{18}O_v$ and $\delta^{18}O_{pv\text{-}eq}$ in our data, the below-cloud evaporation has significant influence on the precipitation isotopic composition. Therefore, it should be cautious to derive the water vapor isotopic composition from the precipitation one.

3.2 Below-cloud processes indicated by ΔdΔδ-diagram

Traditionally, to qualitatively assess the below-cloud evaporation of raindrops, the value of d-excess$_p$ is a benchmark. Due to the differences in diffusivities of the individual water molecules in non-equilibrium fractionation, therefore, it will cause d-excess$_p$ to deviate from 0‰, which is a theoretical value under vapor-liquid equilibrium fractionation at temperatures around 20°C (Gat, 1996). The global mean value of 10‰ for the d-excess$_p$ in precipitation indicates that evaporation is in general a non-equilibrium process. Normally, below-cloud evaporation will decrease d-excess$_p$, and in comparison, mixing with the recycled water vapor from surface evaporation and plant transpiration will increase d-excess$_p$ (Craig, 1961; Dansgaard, 1964). In addition, in the water molecules diffusion process, the water vapor d-excess$_v$ may be modified, and this enhances the uncertainty to gauge the below-cloud evaporation process by solely using d-excess$_p$. In contrast, the ΔdΔδ-diagram introduced by Graf et al. (2019) provides richer information on the below-cloud processes.

Theoretically, on the ΔdΔδ-diagram, Δd<0‰ and Δδ>0‰ indicate the below-cloud evaporation process; Δδ<0‰ represents that the falling raindrop is less influenced by below-cloud evaporation and retains the cloud signals; and Δd and Δδ close to 0‰ suggest equilibrium conditions. By projecting our data on the ΔdΔδ-diagram, the evaporation, equilibration, and non-exchange (e.g., a snowfall event, or a transition from rain to snow with a stronger cloud signal) processes could be clearly differentiated. It is apparent from Fig. 4 that most of the rainfall samples are located in the fourth quadrant with positive $\Delta\delta^{2}H_v$ and negative Δd-excess$_v$, indicating that evaporation is the major below-cloud process. Interestingly, most of the snowfall samples seize the second and third quadrants with negative $\Delta\delta^{2}H_v$, which is suggestive of below-cloud evaporation with less impact on them, and their initial signals are well retained after the cloud-based equilibrium fractionation.

According to the results of numerical simulations and in-situ observations, Graf et al. (2019) summarized that raindrop size and precipitation intensity appear to be the

important driving factors of the below-cloud processes, because raindrops with large diameters and heavy precipitation intensities will reduce their residence time in the atmospheric column, and thereby lower the evaporation possibility during their way down toward the ground surface. However, as for snowfall event, it seems unreasonable to explain the strongly negative $\Delta\delta^2H_v$ by the raindrop size and rain rate (Fig. 4). It is well known that snowfall event happens in low-temperature conditions, and corresponds to weak evaporation, in addition, diffusion speed of the ice phase (solid) to vapor is lower than that of liquid to vapor. Hence, rain/snow formed under such circumstances, their isotopic signals will be less impacted by the environmental factors during its falling. This leads the $\Delta\delta$ to be more negative with the decrease of temperature, such as the phenomenon observed in Graf's et al. (2019) study during the post-frontal periods. Furthermore, on the $\Delta d\Delta\delta$-diagram, the snow samples with positive Δd-excess$_v$ (in the second quadrant) may be related to the supersaturation process, as the liquid has unusually high d-excess$_p$ for the non-equilibrium fractionation of supersaturation (Deshpande et al., 2013; Jouzel and Merlivat, 1984). Our results suggest that in addition to raindrop size and rain rate, precipitation type is also an essential factor that influences the distribution of the data on the $\Delta d\Delta\delta$-diagram.

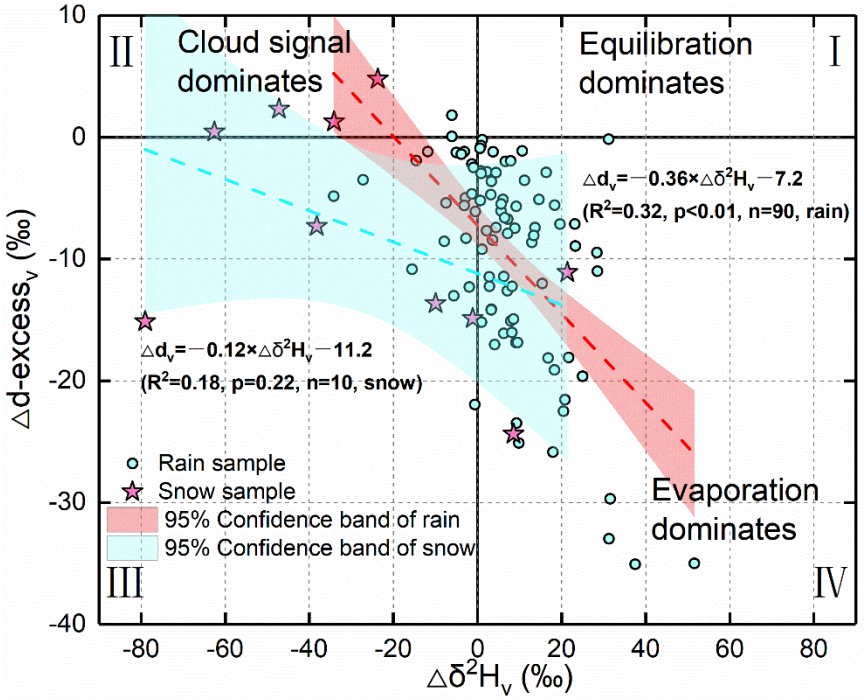

Figure 4 The projection of our data on the suggested $\Delta d\Delta\delta$-diagram by Graf et al. (2019). The solid lines stand for Δd-excess$_v$ and $\Delta\delta^2H_v$ of 0‰. The dashed line corresponds to the linear fit through the samples with the 95% confidence band in shading. The red line is for rainfall samples, and the cyan line is for snowfall samples. The upper Romans represent the category of the quadrant.

In Fig.4, the slope of $\Delta d/\Delta\delta$ is -0.36 for rainfall samples and -0.12 for snowfall samples.

In Graf's et al. (2019) study, they reported a Δd/Δδ slope of -0.3. It should be noted that the slope of Graf's et al. (2019) is based on intra-event samples (from the start to the end of precipitation, each interval of 10 min to collect one sample), while ours is on per-event samples (only collect one sample in each precipitation event). Although the time scale is different in the two studies, interestingly, the rainfall slopes are close to each other, while the snowfall slope is obviously different from the rainfall. The Δd/Δδ slope of -0.3 could represent a general characteristic of rainfall for continental mid-latitude cold front passages (Graf et al., 2019). Xi'an city is located near the 35°N in inland of China, which just belongs to the scope of continental mid-latitude. In comparison, the Δd/Δδ slope of our snow samples is less negative. Therefore, the different Δd/Δδ slopes might be related to the different climatic characteristics or precipitation types. Certainly, to validate this assumption, more works need to be done in future studies.

3.3 Comparing and analyzing the two methods

The ΔdΔδ-diagram provides rich information on the below-cloud processes, but it is only a qualitative analysis. In comparison, the quantitative evaluation is more important to identify the below-cloud evaporation effect. Here, we chose two methods to respectively calculate the variations of $\Delta\delta^2H_p$ and evaporation fraction (F_i) on per-event precipitation, and compared their differences.

3.3.1 Quantitatively evaluate the below-cloud evaporation effect by the two methods

The $\Delta\delta^2H_p$ range from 0 to 131.1 ‰ with an average and standard deviation of 17.8 ± 23.8 ‰, and the F_i range from 0 to 82.7 % with an average and standard deviation of 16.3 ± 21.9 % (n=141) for method 1. The $\Delta\delta^2H_p$ range from -73.8 to 82.5 ‰ with an average and standard deviation of 16.3 ± 24.4‰, and the F_i range from 0 to 67.6 % with an average and standard deviation of 22.1 ± 21.7 % (n=100) for method 2. For the 90 rainfall events with corresponding water vapor data, the average ± standard deviation is 18.4 ± 21.7 ‰ for $\Delta\delta^2H_p$ in method 1, and the value is 18.7 ± 20.6 ‰ for $\Delta\delta^2H_p$ in method 2. For the 10 snowfall events, the average ± standard deviation of $\Delta\delta^2H_p$ is 42.6 ± 43.7 ‰ for method 1 and -6.1 ± 41.6 ‰ for method 2. In the two methods, according to the independent t-test, there are no statistical differences in the $\Delta\delta^2H_p$ of rainfall samples ($F=0$, $p=0.91$, $n=90$), but the $\Delta\delta^2H_p$ of snowfall show a large difference ($F=0.196$, $p<0.05$, $n=10$).

As shown in Fig. 5a and Fig. 5b, the $\Delta\delta^2H_p$ and F_i in the two methods have similar fluctuation trends. The positive $\Delta\delta^2H_p$ and high F_i appear from March to July, while the negative $\Delta\delta^2H_p$ and low F_i show from September to February. In addition, the most positive $\Delta\delta^2H_p$ values are captured by method 1, while the most negative values are detected by method 2. In order to analyze the underlying reason, we checked the equation used to calculate $\Delta\delta^2H_p$. We noted that in eq. 5 the F_r is always lower than 1, and thus (F_r^{β}-1) is negative. Similarly, the $\frac{\gamma}{\alpha}$ is smaller than 1, and thus (1-$\frac{\gamma}{\alpha}$) is also negative. Therefore, the $\Delta\delta^2H_p$ calculated by method 1 could not be a negative number. In method 2, the most negative $\Delta\delta^2H_p$ values are related to the snowfall events. During the supersaturation process, vapor deposition occurs over ice (Jouzel and Merlivat, 1984), which may cause the snow isotopic composition at the ground to be more depleted than its formation height. In fact, the mass of the snow also increases in the supersaturation condition, however, method 1 only considers the evaporation process. The diameter of the raindrop used to determine the terminal velocity and evaporation intensity (Supplemental material, eq. 10-13) does not take into account the snowfall factor which results in great uncertainty in method 1. Therefore, method 1 is not suitable for evaluating the below-cloud effect on the precipitation isotopic composition when the snowfall or low-temperature rainfall events.

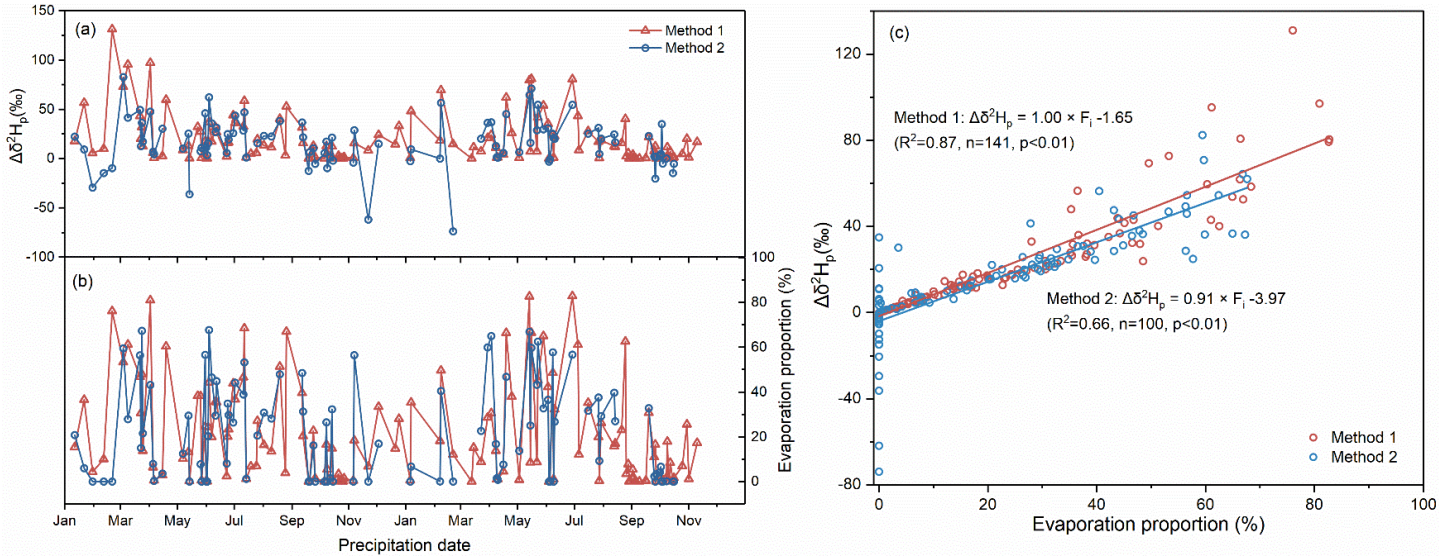

Figure 5 The variation of $\Delta\delta^2H_p$ for per-event precipitation in method 1 and method 2 (a); the same as (a) but for F_i (b); the relationship between F_i and $\Delta\delta^2H_p$ in method 1 and method 2 (c)

In addition, the influence of the below-cloud evaporation effect on the δ^2H_p is heavier in method 1 than in method 2, especially at higher F_i conditions (Fig. 5c), because the slope of $F_i/\Delta\delta^2H$ in method 1 (1.00 ‰/%) is a little steeper than in method 2 (0.91 ‰/%), and the intercept in method 1 (-1.65) is more positive than in method 2 (-3.97). Thus,

under the same evaporation intensity, the $\Delta\delta^2H_p$ is more enriched in method 1 than in method 2.

On the seasonal scale, both methods show that the below-cloud evaporation effect is heavier in spring and summer and weaker in autumn and winter (Fig. S4). Their differences are the smallest in spring and the largest in winter. The significant difference in winter might be related to the supersaturation process.

3.3.2 Meteorological controls on the two methods

To further explore the differences by employing the two methods, we performed the correlation analyses between meteorological factors and the $\Delta\delta^2H_p$ (Fig. 6). The results show that RH is the most important meteorological factor for both methods (Fig. 6b). Although precipitation amounts have influences on both methods as well, their relationships are non-linear or its effect on $\Delta\delta^2H_p$ is rather weak (r=-0.49, method 1; r=-0.30, method2; Fig. 6c). For temperature, in method 1 there is no clear correlation between $\Delta\delta^2H_p$ and temperature (r=0.05), and their positive correlation is weak in method 2 (r=0.42). Wang et al. (2016b) explicitly pointed out that among the parameters of temperature, precipitation amount, RH, and raindrop diameter, RH generally plays a decisive role on Δd-excess in the below-cloud evaporation process.

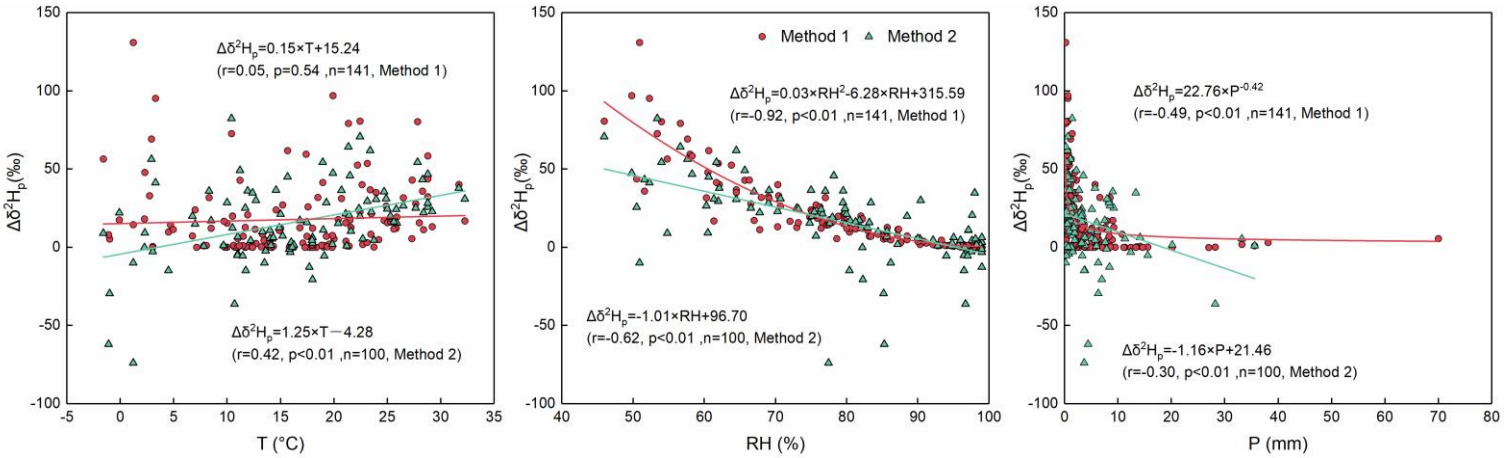

Figure 6 The correlations between the $\Delta\delta^2H_p$ and the temperature in method 1 (red dots) and in method 2 (green triangles) (a); the same as (a) but for RH (b); the same as (a) and (b) but for precipitation amount (c).

In both methods, in an arid environment with high temperature, low RH, and small precipitation amounts the evaporation effect on the $\Delta\delta^2H_p$ is large. However, in the low-temperature conditions (below 5 °C), there is a divergence in $\Delta\delta^2H_p$ for the two methods, which is partly attributed to the supersaturation condition. With the increase

of RH, $\Delta\delta^2H_p$ becomes closer to 0 in both methods, but the variation of $\Delta\delta^2H_p$ is large in method 2 and very limited in method 1 when the RH is higher than 80%. There is a wide range, from 0 to 130 ‰, for $\Delta\delta^2H_p$ when the precipitation amount is small. As the precipitation amount is above 10 mm, the value of $\Delta\delta^2H_p$ tends toward 0 ‰.

3.3.2 Sensitivity test

In method 1, the input physical parameters include temperature, RH, precipitation amount, and surface pressure. In method 2, the input parameters include temperature, RH, and surface pressure. Therefore, these parameters are considered in the sensitivity test.

For the RH test, one case adds 10% to the measured RH, and another case subtracts 10% from the measured RH. If the RH values are above 100%, then they are artificially set to 99% to conform to reality. Two temperature scenarios, plus and minus 10 °C based on the actual temperature, are analyzed. In the sensitivity test of precipitation amount, considering that the amounts are lower than 0.1 mm in some precipitation events, therefore, the reduction lower limit is set at 0.1 mm, and the enhancement upper limit is set at 5 mm. On the basic surface pressure condition, 10 kPa pressure fluctuation is considered for its impact.

As shown in Fig. 7, the increase of RH and precipitation, and decrease of temperature have negative impact, that is, the below-cloud evaporation effect on the isotopic composition will be attenuated. On the contrary, the decrease of RH and precipitation, and increase of temperature have positive impact, indicating that the below-cloud evaporation effect will be strengthened. The varying surface pressure has no impact on the $\Delta\delta^2H_p$ for both methods. Moreover, the influencing strength of the different physical parameters on the $\Delta\delta^2H_p$ is different in the two methods. For example, in method 1, the increase of temperature basically does not change the evaporation effect on the $\Delta\delta^2H_p$, and the influence of decreasing temperature on mitigating evaporation is limited as well. However, the situation is totally different in method 2, where the temperature is a decisive factor. In addition, the influence of RH is over the temperature in method 1, but the condition is reversed in method 2. The precipitation amount is also an important factor, as the influence of precipitation on $\Delta\delta^2H_p$ even surpass the RH when it is increased by 5 mm. Because of the limited decrease in precipitation amount, its positive feedback is hard to evaluate.

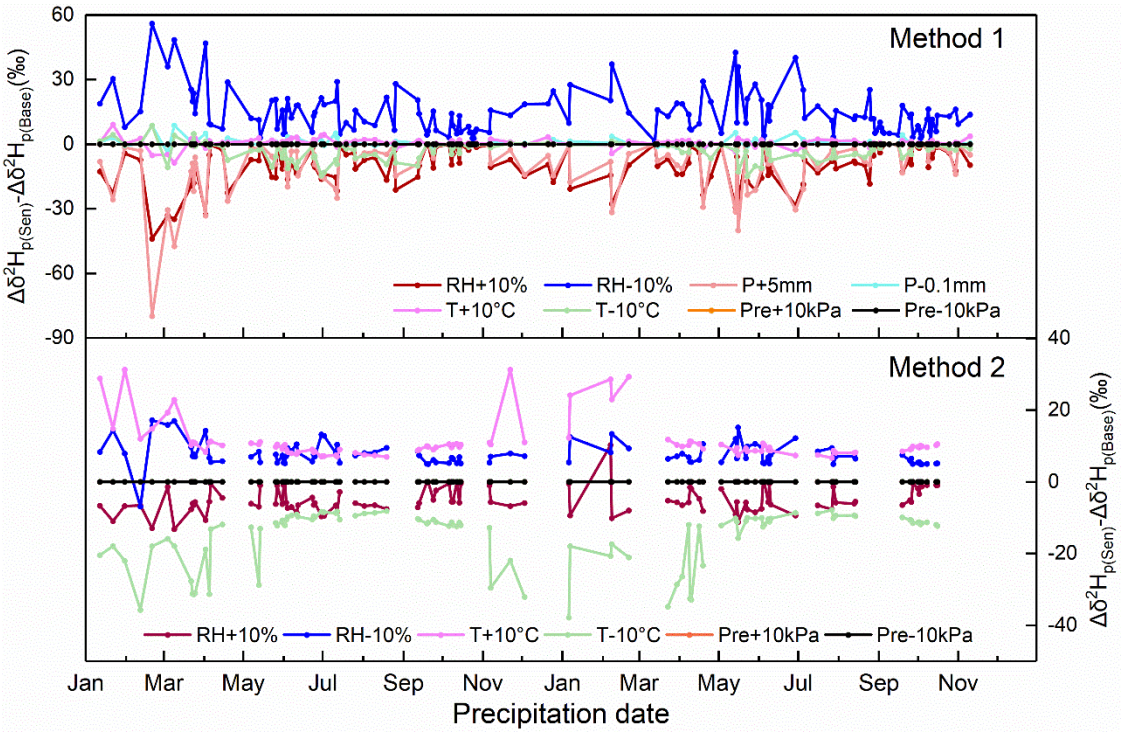

Figure 7 Sensitivity test of $\Delta\delta^2H_p$ under different cases. In method 1, the cases include ± 10% RH, ± 10 °C temperature, ± 10 kPa surface pressure, +5 mm precipitation amount, and -0.1 mm precipitation amount. In method 2, the cases include ± 10% RH, ± 10 °C temperature, and ± 10 kPa surface pressure. The $\Delta\delta^2H_{p(Sen)}$ represents the results of the sensitivity test, and $\Delta\delta^2H_{p(Base)}$ represents the results of the base condition.

In the calculation process of method 2 (eq. 7, and supplemental material, eq. 22), except for the measured ground-level precipitation and water vapor isotopic compositions ($\delta_{gr\text{-}p}$ and $\delta_{gr\text{-}v}$), the other two controlling factors are the equilibrium fractionation factor (α) and the cloud base height. The α is determined by the temperature variations of the cloud base, while the cloud base height is related to surface temperature and RH (supplemental material, eq. 14-17). With RH increase, the cloud base heights decrease, and vice versa (Fig. S5). In comparison, the cloud base heights are not sensitive to the change of temperature (Fig. S5).

Compared with method 2, the calculation process of method 1 is more complex. Many variables, such as raindrop diameter, evaporation intensity, raindrop falling velocity, cloud base height, etc., are needed to be considered, while they are convoluted with temperature, RH, precipitation amount, and surface pressure. Through the sensitivity test, RH and precipitation amount are the two decisive factors in method 1 for deciding the below-cloud evaporation intensity.

3.3.2 Uncertainty estimations

There are many uncertainties in the two methods' estimates. In method 1, the input parameters include the variation of temperature, RH, precipitation amount, and surface pressure. In method 2, the uncertainty comes from the variations of the input temperature, RH, surface pressure, ground level water vapor $\delta^2H_{gr\text{-}v}$, and precipitation δ^2H_p. However, the variations of surface pressure show no impact on the $\Delta\delta^2H_p$ in the sensitivity test, therefore, it is not considered in the uncertainty calculation.

To check the influence of temperature, RH, precipitation amount, and precipitation δ^2H_p on the below-cloud evaporation effect, we assume that the errors are mainly from the measurement uncertainty of the instrument, which is ± 0.3°C, ± 3%, ± 4% precipitation amount, and ± 1.0 ‰, respectively. Due to the humidity effect (section 2.4), the measured $\delta^2H_{gr\text{-}v}$ for each event has a wide range of uncertainty, which varies from 1.3 to 8.2 ‰. Hence, the lower and upper limits of the above input parameters in method 1 and method 2 are used to quantify the uncertainties and add them quadratically (Rangarajan et al., 2017; Wu et al., 2022). We obtain the overall uncertainty varying from 0.71 to 0.72‰ for method 1, and from 0.60 to 1.05‰ for method 2 in the estimates of $\Delta\delta^2H_p$ values (refer to supplemental material, Appendix E)

3.4 The characteristics of below-cloud evaporation effect in Xi'an

Since the below-cloud evaporation is very common in arid and semi-arid regions, before exploring the information contained in the precipitation isotopes, it is important to clearly know the variation of precipitation isotopic composition during its falling. Here, we summarized the seasonal variations of $\Delta\delta^2H_p$ in Xi'an by two methods (Fig. 8).

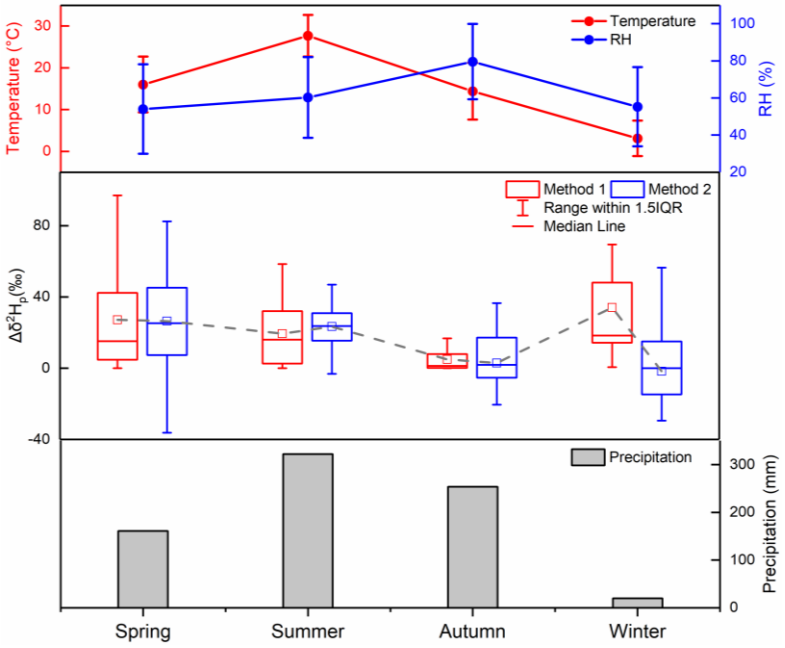

Figure 8 The variations of temperature, RH, precipitation amount, and $\Delta\delta^2H$ in four seasons in Xi'an. In the middle of the figure, the red boxes represent the results from method 1, and the blue boxes represent the results from method 2.

By seasonally dividing the precipitation isotopic composition on the ΔdΔδ-diagram, it shows that samples collected in spring and summer dominate the evaporation phase, reflecting a stronger evaporation influence, while most of the winter precipitation and part of autumn precipitation monopolize the cloud signal phase indicating a weak or no below-cloud evaporation, and even supersaturation on these samples (Fig. S6). Based on quantitative analysis, the two methods show similar evaporation effect in spring, summer, and autumn, and different trends in winter (Fig. 8). The reasons had been discussed in Section 3.3.1. In addition, method 1 shows a narrower variation range of $\Delta\delta^2H_p$ than method 2, because it only considers the below-cloud evaporation process. In method 2, the evaporation effect on δ^2H_p is powerful in spring and summer, and weaker in autumn and winter (Fig. 8). The seasonal variation of $\Delta\delta^2H_p$ basically mirrors the trend of RH. Although the precipitation amount is highest in the summer, the temperature is extremely high and RH is relatively low, which causes the relatively positive $\Delta\delta^2H_p$ in summer. In winter, the low $\Delta\delta^2H$ in method 2 may be related to the precipitation type, because snowfall is the main deposition type in this season.

4 Conclusions

The below-cloud processes of precipitation are complex, variable, and influenced by many factors, especially in arid and semi-arid regions. Previously, below-cloud evaporation is the most well-studied post-condensation process with the aid of the slope of LMWL and d-excess of precipitation. In comparison, other below-cloud processes, such as the vapor-liquid equilibration or the hydrometeors supersaturation growth, have paid less attention to different rain types. In this study, based on the two-year precipitation data collected in Xi'an, we compiled a set of methods to systematically evaluate the below-cloud evaporation effect on local precipitation isotopic composition, and get the following main conclusions:

1. In arid areas, the precipitation and water vapor isotopic compositions have a good relationship, and therefore the joint observation of the two tracers could provide more information on the precipitation processes. In Xi'an, the below-cloud evaporation effect is stronger in spring and summer, and weaker in autumn and winter, and is related to the variation of local RH.

2. Our work validates the general applicability of the ΔdΔδ-diagram. Although there is a difference in timescale between Graf's et al. (2019) study (intra-event) and ours (per-event), the influence of below-cloud processes on our precipitation and water vapor isotopic data can be clearly visualized on the ΔdΔδ-diagram. In this study, the below-cloud evaporation is the main process during the raindrops falling. However, snowfall samples are less influenced by evaporation, and mainly preserve their initial water vapor information. The different Δd/Δδ slopes of rainfall and snowfall might be related to the precipitation types.

3. By comparing the two methods, we find that both could be used to quantitatively evaluate the below-cloud evaporation effect on precipitation except for snowfall events, because there are no statistical differences in their $\Delta\delta^2H_p$ results. The slope of $F_i/\Delta\delta^2H$ in method 1 (1.00 ‰/%) is a little steeper than in method 2 (0.91 ‰/%), indicating the stronger evaporation effect on $\Delta\delta^2H$ for method 1. However, the two methods of $\Delta\delta^2H$ show a large difference in winter, especially for snow samples, which is related to the supersaturation process not being considered in method 1. Through meteorology and sensitivity analysis, RH is the main controlling factor. The two methods show different sensitivity to temperature variations. Through uncertainty estimations, method 2 shows a larger uncertainty range (ranging from 0.60 to 1.05‰) than method 1 (ranging from 0.71 to 0.72‰).

Data availability

The datasets can be obtained from Table S3.

Author contribution

Meng Xing and Weiguo Liu designed the experiments, interpreted the results, and prepared the manuscript with contributions from all co-authors. Meng Xing and Jing Hu analyzed the precipitation and water vapor samples. Jing Hu maintained the experimental instruments.

Competing interests

The authors declare that they have no conflict of interest.

Acknowledgment

This work was supported by Science Foundation of China (No. 42177093), West Light Foundation of The Chinese Academy of Sciences, and China scholarship council. The authors would like to thank Mr. Xijing Cao for helping to collect precipitation samples.

References

Aemisegger, F., Sturm, P., Graf, P., Sodemann, H., Pfahl, S., Knohl, A. and Wernli, H.: Measuring variations of δ 18O and δ 2H in atmospheric water vapour using two commercial laser-based spectrometers: An instrument characterisation study, Atmos. Meas. Tech., 5(7), 1491–1511, doi:10.5194/amt-5-1491-2012, 2012.

Araguás-Araguás, L., Froehlich, K. and Rozanski, K.: Deuterium and oxygen-18 isotope composition of precipitation and atmospheric moisture, Hydrol. Process., 14(8), 1341–1355, doi:10.1002/1099-1085(20000615)14:8<1341::AID-HYP983>3.3.CO;2-Q, 2000.

Bastrikov, V., Steen-Larsen, H. C., Masson-Delmotte, V., Gribanov, K., Cattani, O., Jouzel, J. and Zakharov, V.: Continuous measurements of atmospheric water vapour isotopes in western Siberia (Kourovka), Atmos. Meas. Tech., 7(6), 1763–1776, doi:10.5194/amt-7-1763-2014, 2014.

Benetti, M., Reverdin, G., Pierre, C., Merlivat, L., Risi, C., Steen-Larsen, H. C. and Vimeux, F.: Deuterium excess in marine water vapor: Dependency on relative humidity and surface wind speed during evaporation, J. Geophys. Res., 119(2), 584–593, doi:10.1002/2013JD020535, 2014.

Bowen, G. J., Cai, Z., Fiorella, R. P. and Putman, A. L.: Isotopes in the Water Cycle: Regional- to Global-Scale Patterns and Applications, Annu. Rev. Earth Planet. Sci., 47(1), 453–479, doi:10.1146/annurev-earth-053018-060220, 2019.

Cai, Y., Cheng, H., An, Z., Edwards, R. L., Wang, X., Tan, L. and Wang, J.: Large variations of oxygen isotopes in precipitation over south-central Tibet during Marine Isotope Stage 5, Geology, 38(3), 243–246, doi:10.1130/G30306.1, 2010.

Chakraborty, S., Sinha, N., Chattopadhyay, R., Sengupta, S., Mohan, P. M. and Datye, A.: Atmospheric controls on the precipitation isotopes over the Andaman Islands, Bay of Bengal, Sci. Rep., 6, 19555 [online] Available from: https://doi.org/10.1038/srep19555, 2016.

Christner, E., Aemisegger, F., Pfahl, S., Werner, M., Cauquoin, A., Schneider, M., Hase, F., Barthlott, S. and Schädler, G.: The Climatological Impacts of Continental Surface Evaporation, Rainout, and Subcloud Processes on δD of Water Vapor and Precipitation in Europe, J. Geophys. Res. Atmos., 123(8), 4390–4409, doi:10.1002/2017JD027260, 2018.

Clark, I. D. and Fritz, P.: Environmental Isotopes in Hydrogeology, Lewis, Boca Raton, Florida., 1997.

765 Craig, H.: Isotopic Variations in Meteoric Waters, Science (80-.)., 133(3465), 1702–1703, 1961.
766 Dansgaard, W.: Stable isotopes in precipitation, Tellus, 16(4), 436–468,
767 doi:10.3402/tellusa.v16i4.8993, 1964.
768 Deshpande, R. D., Maurya, A. S., Kumar, B., Sarkar, A. and Gupta, S. K.: Rain-vapor
769 interaction and vapor source identification using stable isotopes from semiarid western India, J.
770 Geophys. Res. Atmos., 115(23), 1–11, doi:10.1029/2010JD014458, 2010.
771 Deshpande, R. D., Maurya, A. S., Kumar, B., Sarkar, A. and Gupta, S. K.: Kinetic fractionation
772 of water isotopes during liquid condensation under super-saturated condition, Geochim.
773 Cosmochim. Acta, 100, 60–72, doi:https://doi.org/10.1016/j.gca.2012.10.009, 2013.
774 Fiorella, R. P., Bares, R., Lin, J. C., Ehleringer, J. R. and Bowen, G. J.: Detection and variability
775 of combustion-derived vapor in an urban basin, Atmos. Chem. Phys., 18(12), 8529–8547,
776 doi:10.5194/acp-18-8529-2018, 2018.
777 Fisher, D. A.: Remarks on the deuterium excess in precipitation in cold regions, Tellus B, 43(5),
778 401–407, doi:https://doi.org/10.1034/j.1600-0889.1991.t01-4-00006.x, 1991.
779 Froehlich, K., Kralik, M., Papesch, W., Rank, D., Scheifinger, H. and Stichler, W.: Deuterium
780 excess in precipitation of Alpine regions – moisture recycling, Isotopes Environ. Health Stud.,
781 44(1), 61–70, doi:10.1080/10256010801887208, 2008.
782 Gat, J. R.: OXYGEN AND HYDROGEN ISOTOPES IN THE HYDROLOGIC CYCLE, Annu.
783 Rev. Earth Planet. Sci., 24(1), 225–262, doi:10.1146/annurev.earth.24.1.225, 1996.
784 Gorski, G., Strong, C., Good, S. P., Bares, R., Ehleringer, J. R. and Bowen, G. J.: Vapor
785 hydrogen and oxygen isotopes reflect water of combustion in the urban atmosphere, Proc. Natl.
786 Acad. Sci., 112(11), 3247–3252, doi:10.1073/pnas.1424728112, 2015.
787 Graf, P., Wernli, H., Pfahl, S. and Sodemann, H.: A new interpretative framework for below-
788 cloud effects on stable water isotopes in vapour and rain, Atmos. Chem. Phys., 19(2), 747–765,
789 doi:10.5194/acp-19-747-2019, 2019.
790 Guan, H., Zhang, X., Skrzypek, G., Sun, Z. and Xu, X.: Deuterium excess variations of rainfall
791 events in a coastal area of south Australia and its relationship with synoptic weather systems
792 and atmospheric moisture sources, J. Geophys. Res. Atmos., 118(2), 1123–1138,
793 doi:10.1002/jgrd.50137, 2013.
794 Jacob, H. and Sonntag, C.: An 8-year record of the seasonal variation of 2 H and 18 O in
795 atmospheric water vapour and precipitation at Heidelberg, Germany, Tellus B Chem. Phys.
796 Meteorol., 43(3), 291–300, doi:10.3402/tellusb.v43i3.15276, 1991.
797 Jeelani, G., Deshpande, R. D., Galkowski, M. and Rozanski, K.: Isotopic composition of daily
798 precipitation along the southern foothills of the Himalayas: Impact of marine and continental
799 sources of atmospheric moisture, Atmos. Chem. Phys., 18(12), 8789–8805, doi:10.5194/acp-
800 18-8789-2018, 2018.
801 Jouzel, J. and Merlivat, L.: Deuterium and oxygen 18 in precipitation: Modeling of the isotopic
802 effects during snow formation, J. Geophys. Res., 89(D7), 11749, doi:10.1029/jd089id07p11749,
803 1984.
804 Jouzel, J., Delaygue, G., Landais, A., Masson-Delmotte, V., Risi, C. and Vimeux, F.: Water

isotopes as tools to document oceanic sources of precipitation, Water Resour. Res., 49(11), 7469–7486, doi:https://doi.org/10.1002/2013WR013508, 2013.
Li, L. and Garzione, C. N.: Spatial distribution and controlling factors of stable isotopes in meteoric waters on the Tibetan Plateau : Implications for paleoelevation reconstruction, Earth Planet. Sci. Lett., 460, 302–314, doi:10.1016/j.epsl.2016.11.046, 2017.
Li, Z., Qi, F., Wang, Q. J., Kong, Y., Cheng, A., Song, Y., Li, Y., Li, J. and Guo, X.: Contributions of local terrestrial evaporation and transpiration to precipitation using δ 18 O and D-excess as a proxy in Shiyang inland river basin in China, Glob. Planet. Chang., 146, 140–151, 2016.
Liu, W., Feng, X., Liu, Y., Zhang, Q. and An, Z.: δ18O values of tree rings as a proxy of monsoon precipitation in arid Northwest China, Chem. Geol., 206(1), 73–80, doi:https://doi.org/10.1016/j.chemgeo.2004.01.010, 2004.
Liu, W., Liu, H., Wang, Z., An, Z. and Cao, Y.: Hydrogen isotopic compositions of long-chain leaf wax n-alkanes in Lake Qinghai sediments record palaeohydrological variations during the past 12 ka, Quat. Int., 449, 67–74, doi:https://doi.org/10.1016/j.quaint.2017.05.024, 2017a.
Liu, W., Wang, H., Leng, Q., Liu, H., Zhang, H. and Xing, M.: Hydrogen isotopic compositions along a precipitation gradient of Chinese Loess Plateau : Critical roles of precipitation / evaporation and vegetation change as controls for leaf wax δ D, Chem. Geol., 528(April), 119278, doi:10.1016/j.chemgeo.2019.119278, 2019.
Liu, Y., Liu, H., Song, H., Li, Q., Burr, G. S., Wang, L. and Hu, S.: A monsoon-related 174-year relative humidity record from tree-ring δ18O in the Yaoshan region, eastern central China, Sci. Total Environ., 593–594, 523–534, doi:https://doi.org/10.1016/j.scitotenv.2017.03.198, 2017b.
Merlivat, L. and Jouzel, J.: Global climatic interpretation of the deuterium-oxygen 18 relationship for precipitation, J. Geophys. Res. Ocean., 84(C8), 5029–5033, doi:https://doi.org/10.1029/JC084iC08p05029, 1979.
Peng, T. R., Liu, K. K., Wang, C. H. and Chuang, K. H.: A water isotope approach to assessing moisture recycling in the island-based precipitation of Taiwan: A case study in the western Pacific, Water Resour. Res., 47(8), 1–11, doi:10.1029/2010WR009890, 2011.
Putman, A. L., Fiorella, R. P., Bowen, G. J. and Cai, Z.: A Global Perspective on Local Meteoric Water Lines-SM, Water Resour. Res., 1–6, doi:10.1351/pac198961081483.Jaffey, 2019a.
Putman, A. L., Fiorella, R. P., Bowen, G. J. and Cai, Z.: A Global Perspective on Local Meteoric Water Lines: Meta-analytic Insight into Fundamental Controls and Practical Constraints, Water Resour. Res., 2019WR025181, doi:10.1029/2019WR025181, 2019b.
Rangarajan, R., Laskar, A. H., Bhattacharya, S. K., Shen, C. C. and Liang, M. C.: An insight into the western Pacific wintertime moisture sources using dual water vapor isotopes, J. Hydrol., 547, 111–123, doi:10.1016/j.jhydrol.2017.01.047, 2017.
Salamalikis, V., Argiriou, A. A. and Dotsika, E.: Isotopic modeling of the sub-cloud evaporation effect in precipitation, Sci. Total Environ., 544, 1059–1072, doi:10.1016/j.scitotenv.2015.11.072, 2016.
Salmon, O. E., Welp, L. R., Baldwin, M. E., Hajny, K. D., Stirm, B. H. and Shepson, P. B.: Vertical profile observations of water vapor deuterium excess in the lower troposphere, Atmos.

Chem. Phys., 19(17), 11525–11543, doi:10.5194/acp-19-11525-2019, 2019.
Steen-Larsen, H. C., Johnsen, S. J., Masson-Delmotte, V., Stenni, B., Risi, C., Sodemann, H., Balslev-Clausen, D., Blunier, T., Dahl-Jensen, D., Ellehøj, M. D., Falourd, S., Grindsted, A., Gkinis, V., Jouzel, J., Popp, T., Sheldon, S., Simonsen, S. B., Sjolte, J., Steffensen, J. P., Sperlich, P., Sveinbjörnsdóttir, A. E., Vinther, B. M. and White, J. W. C.: Continuous monitoring of summer surface water vapor isotopic composition above the Greenland Ice Sheet, Atmos. Chem. Phys., 13(9), 4815–4828, doi:10.5194/acp-13-4815-2013, 2013.
Stewart, M. K.: Stable isotope fractionation due to evaporation and isotopic exchange of falling waterdrops: Applications to atmospheric processes and evaporation of lakes, J. Geophys. Res., 80(9), 1133–1146, doi:10.1029/JC080i009p01133, 1975.
Sun, C., Chen, W., Chen, Y. and Cai, Z.: Stable isotopes of atmospheric precipitation and its environmental drivers in the Eastern Chinese Loess Plateau , China, J. Hydrol., 581(November 2019), 124404, doi:10.1016/j.jhydrol.2019.124404, 2020.
Tan, L., An, Z., Huh, C.-A., Cai, Y., Shen, C.-C., Shiau, L.-J., Yan, L., Cheng, H. and Edwards, R. L.: Cyclic precipitation variation on the western Loess Plateau of China during the past four centuries, Sci. Rep., 4(1), 6381, doi:10.1038/srep06381, 2014.
Thompson, L. G., Yao, T., Mosley-Thompson, E., Davis, M. E., Henderson, K. A. and Lin, P.-N.: A High-Resolution Millennial Record of the South Asian Monsoon from Himalayan Ice Cores, Science (80-.)., 289(5486), 1916 LP – 1919, doi:10.1126/science.289.5486.1916, 2000.
Tian, C., Wang, L., Kaseke, K. F. and Bird, B. W.: Stable isotope compositions (δ 2 H , δ 18 O and δ 17 O) of rainfall and snowfall in the central United States, Sci. Rep., (October 2017), 1–15, doi:10.1038/s41598-018-25102-7, 2018.
Wan, H., Liu, W. and Xing, M.: Isotopic composition of atmospheric precipitation and its tracing significance in the Laohequ Basin, Loess plateau, China, Sci. Total Environ., 640–641(May), 989–996, doi:10.1016/j.scitotenv.2018.05.338, 2018.
Wang, S., Zhang, M., Che, Y., Chen, F. and Fang, Q.: Contribution of recycled moisture to precipitation in oases of arid central Asia: A stable isotope approach, Water Resour. Res., 52(4), 3246–3257, doi:10.1002/2015WR018135, 2016a.
Wang, S., Zhang, M., Che, Y., Zhu, X. and Liu, X.: Influence of Below-Cloud Evaporation on Deuterium Excess in Precipitation of Arid Central Asia and Its Meteorological Controls, J. Hydrometeorol., 17(7), 1973–1984, doi:10.1175/JHM-D-15-0203.1, 2016b.
Wang, S., Zhang, M., Hughes, C. E., Crawford, J., Wang, G., Chen, F., Du, M., Qiu, X. and Zhou, S.: Meteoric water lines in arid Central Asia using event-based and monthly data, J. Hydrol., 562(May), 435–445, doi:10.1016/j.jhydrol.2018.05.034, 2018a.
Wang, Z., An, Z., Liu, Z., Qiang, X., Zhang, F. and Liu, W.: Hydroclimatic variability in loess δDwax records from the central Chinese Loess Plateau over the past 250 ka, J. Asian Earth Sci., 155, 49–57, doi:https://doi.org/10.1016/j.jseaes.2017.11.008, 2018b.
Welp, L. R., Lee, X., Kim, K., Griffis, T. J., Billmark, K. A. and Baker, J. M.: δ18O of water vapour, evapotranspiration and the sites of leaf water evaporation in a soybean canopy, Plant, Cell Environ., 31(9), 1214–1228, doi:10.1111/j.1365-3040.2008.01826.x, 2008.

Wen, X. F., Zhang, S. C., Sun, X. M., Yu, G. R. and Lee, X.: Water vapor and precipitation isotope ratios in Beijing, China, J. Geophys. Res. Atmos., 115(1), 1–10, doi:10.1029/2009JD012408, 2010.

Wu, H., Fu, C., Zhang, C., Zhang, J., Wei, Z. and Zhang, X.: Temporal Variations of Stable Isotopes in Precipitation from Yungui Plateau: Insights from Moisture Source and Rainout Effect, J. Hydrometeorol., 23(1), 39–51, doi:10.1175/JHM-D-21-0098.1, 2022.

Wu, J., Li, P. and Qian, H.: Variation characteristics of meteorological elements and prediction model of available precipitation in Xi'an city, South-to-North water Transf. water Sci. Technol., 11(001), 50–54, 2013.

Xing, M., Liu, W., Li, X., Zhou, W., Wang, Q., Tian, J., Li, X., Tie, X., Li, G., Cao, J., Bao, H. and An, Z.: Vapor isotopic evidence for the worsening of winter air quality by anthropogenic combustion-derived water, Proc. Natl. Acad. Sci., 117(52), 33005–33010, doi:10.1073/pnas.1922840117, 2020.

Yao, T., Thompson, L. G., Mosley-Thompson, E., Zhihong, Y., Xingping, Z. and Lin, P.-N.: Climatological significance of δ18O in north Tibetan ice cores, J. Geophys. Res. Atmos., 101(D23), 29531–29537, doi:10.1029/96JD02683, 1996.

Yao, T., Masson-Delmotte, V., Gao, J., Yu, W., Yang, X., Risi, C., Sturm, C., Werner, M., Zhao, H., He, Y., Ren, W., Tian, L., Shi, C. and Hou, S.: A review of climatic controls on δ18O in precipitation over the Tibetan Plateau: Observations and simulations, Rev. Geophys., 51(4), 525–548, doi:10.1002/rog.20023, 2013.

Zhao, L., Liu, X., Wang, N., Kong, Y., Song, Y., He, Z., Liu, Q. and Wang, L.: Contribution of recycled moisture to local precipitation in the inland Heihe River Basin, Agric. For. Meteorol., 271(July 2018), 316–335, doi:10.1016/j.agrformet.2019.03.014, 2019.

Zhu, G. F., Li, J. F., Shi, P. J., He, Y. Q., Cai, A., Tong, H. L., Liu, Y. F. and Yang, L.: Relationship between sub-cloud secondary evaporation and stable isotope in precipitation in different regions of China, Environ. Earth Sci., 75(10), 876, 2016.